

A LARGE AND FAINT PHOTOMETRIC CATALOG ON THE ECLIPTIC

MARC W. BUIE¹, DAVID E. TRILLING², LAWRENCE H. WASSERMAN³, AND RICHARD A. CRUDO⁴

¹ Southwest Research Institute, 1050 Walnut St., Suite 300, Boulder, CO 80302, USA; buie@boulder.swri.edu

² Department of Physics and Astronomy, Northern Arizona University, Flagstaff, AZ, USA; david.trilling@nau.edu

³ Lowell Observatory, 1400 W. Mars Hill Rd., Flagstaff, AZ 86001, USA; lh@lowell.edu

⁴ George Washington University Law School, George Washington University; rcrudo@gmail.com

Received 2011 January 18; accepted 2011 April 18; published 2011 May 27

ABSTRACT

A photometric catalog, developed for the calibration of the Deep Ecliptic Survey, is presented. The catalog contains 213,272 unique sources that were measured in V and R filters and transformed to the Johnson–Cousins systems using the Landolt standard catalog. All of the sources lie within 6° of the ecliptic and cover all longitudes except for the densest stellar regions nearest the galactic center. Seventeen percent of the sources in the catalog are derived from three or more nights of observation. The catalog contains sources as faint as $R \sim 19$ but the largest fraction fall in the $R \sim 15\text{--}16$ ($V \sim 16\text{--}17$) mag range. All magnitude bins down to $R = 19$ have a significant fraction of objects with uncertainties ≤ 0.1 mag.

Key words: catalogs – Kuiper belt: general – stars: general – techniques: photometric

Online-only material: color figures, machine-readable tables

1. INTRODUCTION

The Deep Ecliptic Survey (DES) was a project started in 1998 to survey the outer solar system near the ecliptic plane. This project was granted NOAO Survey status in 2000 and covered more than 800 deg^2 through the end of its observational phase in 2005.

Some notable results of the DES are the discovery of 870 trans- or ultra-neptunian objects (hereafter referred to as TNOs), of which 498 have received at least provisional designations from the Minor Planet Center. Of these, 326 objects have well-determined orbits as of 2010 December. These distant objects span the full gamut of dynamical classes currently seen in the outer solar system. This includes objects that are in various mean motion resonances with Neptune, classical TNOs that are in low- e and low- i orbits located roughly between 42 and 45 AU, and numerous examples of excited or scattered objects. More information about earlier results can be found in the first two key survey papers (Millis et al. 2002; Elliot et al. 2005).

The results of the DES have already been extensively used as target lists for several follow-on surveys such as the *Hubble Space Telescope* (HST) TNO binary survey (Stephens & Noll 2006) and the *Spitzer Space Telescope* thermal survey (Brucker et al. 2009). We expect these results to continue to be of value, especially once the final survey results are published.

One key goal of the survey is to provide a photometrically well-calibrated set of images, primarily in the form of limiting magnitudes, as well as objects with good apparent brightness measurements at the time of discovery. The search observations were all taken with the NOAO 4 m telescopes at Kitt Peak and Cerro Tololo using the Mosaic cameras resident on each. The observational cadence was designed to maximize the number of objects discovered given this instrumentation. No time was given over to photometric calibration during the survey observations. Therefore, to get photometrically calibrated survey data we used other, smaller telescopes to collect the necessary photometric support data. This paper describes that photometric calibration effort in detail while also making the final photometric catalog available. We expect that this catalog will be useful

for many purposes beyond the DES, as this catalog is substantially deeper than the Landolt catalogs and does not overlap with regions calibrated by the Sloan Digital Sky Survey (SDSS).

Under good conditions, the survey data reached a limiting magnitude $R = 23.5\text{--}24$. The saturation limit for these data was typically $R \sim 17$ though this limit varies with image quality and sky transparency. The survey observations used a few different filters over the course of the project. The bulk of the observations were collected with a VR filter (NOAO Bernstein VR Broad, k1040) designed to maximize the detected photons from these solar-type objects while minimizing the amount of sky background, particularly from OH emission in the red end of the CCD wavelength range. This filter was not available for the entire survey. The first observations were taken with no filter at all and we used an SDSS r' filter for a short time as well.

The search region for the DES was limited to $\pm 6^\circ$ from the ecliptic. Additional details about how the survey was setup can be found in Millis et al. (2002). Of the 3561 defined fields for the survey, 1943 were used and require calibration. During the survey, we needed to recover our newly discovered objects but the follow-up objects often landed outside the range of our usable fields. In all, there were 1215 of these recovery fields needing calibration.

We have chosen to make the final photometric calibration for the survey in the SDSS $ugriz$ system. This decision was based on the availability of the SDSS photometric catalog (Adelman-McCarthy et al. 2006). Roughly 30% of our survey images could be directly calibrated with SDSS data thus requiring no additional effort on our part. The search and follow-up fields without absolutely calibrated reference stars are the target of this work. Note that the SDSS fluxes we report here are largely to document the absolute calibration of the DES. Our measured V , R , and $(V - R)$ magnitudes remain the primary result of this work and there will likely be improvements to transformation that will change the SDSS magnitudes.

2. OBSERVATIONS

The observing program described here was designed to collect data for calibrating the DES. The final goal was to

Table 1
List of Field Centers

Field	R.A. (J2000)	Decl.	Dates
F00005	23:59:40.121	+03:42:03.36	041103 041104 071124
F00006	00:00:29.267	+03:04:45.75	
F00008	00:00:17.848	+01:48:51.51	011117 040731 040809 071027 080906
F00018	00:00:10.256	−04:12:19.00	071204 080913 081015
F12586	23:58:07.385	+02:08:58.68	011120 040903 040907 071102 080913
F12597	23:58:11.635	−04:21:38.72	
FF0000	08:14:32.305	+20:24:35.14	091103 091104 091124
FF0001	09:05:51.420	+16:16:58.63	091124 091125 091126
FF0002	10:34:58.260	+10:03:24.36	
FF0003	12:40:27.597	−05:18:40.07	090402 090403 090405
FF0004	22:42:00.020	−07:38:14.76	
FF0005	22:55:56.000	−07:48:23.29	091009 091023 091026

(This table is available in its entirety in a machine-readable form in the online journal. A portion is shown here for guidance regarding its form and content.)

Table 2
Nightly Photometric Transformation Coefficients

Date	Inst.	Fil	C ₁	C ₂	<i>k</i>	σ_k	F _{<i>k</i>}	ϵ	σ_ϵ	F _{ϵ}	η	σ_η	F _{η}	JDref	Z	σ_Z	F _Z	N	χ^2
2001 Aug 26	PCCD	R	V	R	0.12653	0.00695	0	−0.0820	0.0090	0	0.00000	0.00000	1	2452147.65917	−2.411	0.015	0	15	1.75
2001 Aug 26	PCCD	V	V	R	0.17364	0.00958	0	−0.0263	0.0188	0	0.00000	0.00000	1	2452147.65938	−2.618	0.022	0	20	1.84
2005 Feb 4	SITE2k	R	V	R	0.10028	0.00177	0	0.0503	0.0029	0	0.00000	0.00000	1	2453405.83331	−0.418	0.003	0	106	5.53
2005 Feb 4	SITE2k	V	V	R	0.14684	0.00137	0	0.0318	0.0027	0	0.00000	0.00000	1	2453405.83250	−0.581	0.003	0	115	4.80
2006 Feb 27	ccd21big	R	V	R	0.09023	0.00204	0	−0.0357	0.0035	0	−0.00193	0.00018	0	2453793.81436	0.827	0.004	0	168	7.68
2006 Feb 27	ccd21big	V	V	R	0.12390	0.00258	0	−0.0113	0.0042	0	−0.00251	0.00023	0	2453793.81426	0.808	0.005	0	175	8.12
2006 Apr 7	SMARTS	R	V	R	0.06500	0.00579	0	0.0122	0.0036	0	0.00000	0.00000	1	2453832.63795	−0.633	0.007	0	148	4.63
2006 Apr 7	SMARTS	V	V	R	0.10866	0.00414	0	0.0514	0.0032	0	0.00000	0.00000	1	2453832.62279	−0.608	0.005	0	144	3.46
2007 Oct 8	NASAcam	R	V	R	0.08276	0.00140	0	−0.1238	0.0033	0	0.00000	0.00000	1	2454381.87503	−1.259	0.003	0	179	4.28
2007 Oct 8	NASAcam	V	V	R	0.12537	0.00188	0	−0.0915	0.0042	0	0.00000	0.00000	1	2454381.87503	−1.193	0.004	0	132	3.78

Notes. “Date” is the UT date of observation. “Inst.” is the name of the instrument. “Fil” is the filter used for the observation. The color used in transformation is “C₁” – “C₂.” *k*, ϵ , η , and Z are the transformation coefficients as defined in Equation (1). Each of these quantities is followed by its uncertainty (σ) and a flag that indicates if the term was fitted (0) or forced (1). “JDref” is the reference time used for the time-variable extinction term. “N” is the total number of standard star measurements used to constrain the solution. “ χ^2 ” shows the goodness-of-fit statistic prior to the a posteriori adjustment.

(This table is available in its entirety in a machine-readable form in the online journal. A portion is shown here for guidance regarding its form and content.)

get fluxes in the SDSS photometric system but those filters were not available. Instead we used Johnson–Cousins filters for our observations with the expectation of transforming these measurements to the SDSS system. With the brightness range of the DES in mind we designed the observing protocol such that $R = 17$ would have a signal-to-noise ratio of 100:1. This choice ensures a range of stellar magnitudes that overlaps the brightness range captured by the DES. To find a suitable calibration star, we took the center 19.2×19.2 arcmin of each MOSAIC field and searched the USNO B1.0 catalog for the brightest star fainter than 17th mag within that field. The coordinate of that star became the center of a calibration field.

Table 1 provides all the defined calibration field centers along with the date each field was observed. All of the field names starting with a single “F” match the names of the corresponding survey field. The field names starting with “FF” are calibration fields for the follow-up observations. The “F” fields are ordered in increasing right ascension while the order for “FF” fields is random along the ecliptic.

In all, four different telescopes were used to collect the photometric data presented here. The largest contribution was made by the Lowell Observatory 0.8 m telescope. Additional contributions were made by the SMARTS 0.9 m telescope, the University of Arizona 1.5 m Kuiper Telescope, and the Lowell Observatory 1.2 m Hall telescope. At all facilities,

standard Johnson–Cousins V and R filters were used to collect the raw photometric data. Multiple exposures (3–5) per filter were collected for each field and the images always alternated between filters to obtain the full set of data (e.g., RVRVR...).

The goal of this project was to get three nights of data per field under photometric conditions. Table 2 contains a listing of the good observing nights for this project. Also contained in the listing are the transformation coefficients derived for each night.

2.1. Lowell Observatory 0.8 m Telescope

This telescope was converted to fully autonomous operation in 2000. Full details of this system and the cameras used can be found in Buie (2010). All data taken from 2000 to 2006 were collected with the PCCD camera with a field of view of 7×9 arcmin and a pixel scale of 1.23 arcsec pixel^{−1}. The data from 2007 to 2010 were collected with the NASAcam instrument with a much larger 16 arcmin field of view and a pixel scale of 0.46 arcsec pixel^{−1}. This telescope has a focus that depends very strongly on temperature, thus requiring frequent focus operations. Typical seeing for this facility is 3”–4”, though once the seeing gets to the low end of the range there is a problem with the tracking that leads to variable amounts of trailing. When the seeing is at or above 4” this trailing is not evident.

The observing cadence for this project was governed by a customized program that built a specific observing script for the entire night. For each night of observing a decision was made based on the weather forecast shortly before sunset. If the night had a reasonable chance of being photometric, the night's observing script would be built in a matter of seconds, transferred over the network to the robotic system, and loaded for execution.

The script for each night was built based on a consistent set of observing requirements. First, all fields that were candidates for scheduling were loaded from the central coordinating file. Only those fields that could be reached above 2.5 airmasses sometime in the night were kept for further consideration. Also, DES calibration fields and standard star fields within 30° of the moon were excluded from consideration.

Building the nightly script starts with commands to wait for sunset and initialize and prepare the telescope for observing (e.g., open the dome, initialize focus). Then, the system would pause until it became dark enough to begin observing. This allows time for the dome and telescope to cool off before the start of observations.

When the sun reaches an elevation of -8° the system verifies the pointing of the telescope using a magnitude 1–2 star. The star will always be saturated but the chances of confusion with the wrong star are effectively zero. A rough measurement of focus is collected at a solar elevation of -9° . Science observations begin when the solar elevation reaches $-9:5$.

Through the night the schedule is built by deciding what is the best observation to do at any given time, with no look back or look ahead. At each decision time there are three choices: either focus the telescope, collected standard star observations, or collect science data. When an observation is added to the schedule, an estimate of the elapsed time for that observation is added to the time counter. The schedule is built, one block at a time until the solar elevation becomes greater than $-9:5$. The night is closed out by collecting flat field, dark, and bias images as needed.

Focusing the telescope has the highest priority. If the time since the last focus is greater than 1.2 hr, a focus observation is placed in the schedule. The focus procedure will not work on an arbitrarily bad state of focus. For fast operation, we must assume that the optimal focus is close to the current position. A small but meaningful change in focus is 10 units for this system. We scan ± 100 units about the current focus. The cadence for focusing is set to ensure the largest possible change in focus is less than 100 units. Normal changes in focus position were typically 10–20 units which translates to a change in point-spread function (PSF) of $\sim 10\%$. The PSF width changed by a factor of two over the range of focus position tested. Buie (2010) contains more information about the focus methodology.

The second highest priority was to make regular observations of Landolt standard fields (Landolt 1992) in blocks where one field is observed at 2.5 airmasses and the other near the meridian. Standard fields blocks were observed as close as possible to a 2 hr cadence limited by actual field availability and avoiding the moon. Sometimes a third intermediate airmass field was included as well. An extended discussion of designing and scheduling standard star observations can be found in Buie (2010).

The science data are then scheduled when it is not time for either focus or standard stars. Of all the candidate fields for the night, the one closest to the meridian is chosen. The execution time was 20 minutes for a single calibration field.

2.2. Lowell Observatory 1.2 m Hall Telescope

We used the Hall telescope for a small number of nights. This system was operated in a conventional, manually operated mode. The detector was an SITe 2048×2048 detector at the cassegrain focus with a remotely operated filter wheel. All data were binned 2×2 to reduce the readout time to roughly 1 minute. The binned image scale was $1.18 \text{ arcsec pixel}^{-1}$. The field of view for this camera is roughly 24 arcmin and the seeing is marginally better than the 0.8 m telescope. Despite the slightly larger aperture and slightly better seeing, this telescope returned less useful data per night than the smaller telescope. This was caused in equal measure by the long readout time and the manual operation mode. Because of its relative effectiveness and cost of operation, this facility was not used very much even though it could have helped significantly reduce the time span of the data collection process.

The observing protocol was essentially the same as for the 0.8 m telescope with the exception of focusing the telescope. This system took 10–15 minutes to precisely determine focus and this was done only at the start of each run. The adverse impact of this decision was not very important, though. The secondary support and control for this telescope was recently redesigned with the result that focus is almost completely independent of temperature and it was reasonable to assume that the focus would not change as long as the instrument and telescope were not disturbed as is the case during a single observing run.

2.3. SMARTS Telescope

We were awarded 10 nights on the NOAO/CTIO/SMARTS 0.9 m telescope in the 2005B and 2006A semesters. All of the 2005B nights were lost to heavy clouds. All five of the 2006A nights were useful and data were obtained by service observer Alberto Miranda. The detector is a Tek 2 K \times 2 K device at the Cassegrain focus with an image scale of $0.4 \text{ arcsec pixel}^{-1}$. The field of view is 13.7 arcmin on a side and exposure times were 60 s. Typical seeing was 1–2 arcsec. A total of 130 fields were observed under photometric conditions with this telescope.

2.4. University of Arizona 1.5 m Kuiper Telescope

We were awarded 25 nights on the Steward Observatory 1.54 m (61 inch) Kuiper telescope on Mt. Bigelow, Arizona, between 2004 December and 2006 May. This telescope is operated only in classical user mode. Useful data were acquired with Steward Observatory's "2KBigCCD" device (also known as "ccd21big"), with a field of view of 14.5 arcmin square and a 3×3 binned image scale of $1.24 \text{ arcsec pixel}^{-1}$. Typical seeing was 3–4 arcsec for these data and all exposures were 60 s. A total of 432 fields were observed under photometric conditions with this telescope.

3. REDUCTIONS

The same set of steps were applied to all data for the project once the image calibration was completed (e.g., flat fielding). This section describes how we proceed from image data to individual source flux measurements.

3.1. Nightly Processing

Each night was processed as a stand-alone group of data. First, a photometric aperture was chosen for the night according to the seeing and image quality for that night. All photometric

extractions using aperture summation follow the methodology described in Buie & Bus (1992) using `basphote.pro`, a routine from Buie’s IDL library.⁵ One recent enhancement of our photometric extraction technique is to include the readout noise of the detector in the propagation of errors into the instrumental magnitude. The typical size of the object aperture was about $2.5 \times \text{FWHM}$. The sky aperture was quite large. The inner sky annulus radius was always set to 10 pixels larger than the object aperture. The outer sky annulus radius depended on the instrument but was usually at least 150 pixels. The sky signal was determined from the robust mean of the pixels falling in the sky annulus, using `robomean.pro`. This routine can automatically exclude all pixels that are contaminated by field stars, cosmic ray strikes, or any other image defects.

The Landolt standard fields were processed first and used to determine the transformation coefficients for the night. The transformation relationship we use is

$$M = m - kX + \epsilon C - \eta(t - t_0)X + Z, \quad (1)$$

where M is the standard magnitude, m is the instrumental magnitude, k is the extinction coefficient, X is the airmass, ϵ is the color coefficient, C is the standard color for the object, η is the time-dependent extinction coefficient, t is the time of observation, t_0 is the reference time for night, and Z is the zero point. The reference time is the mean time for all standard star measurements in the night. In the fitting software we can choose to either fit a given term or force an explicit value on the solution. For the best nights we fit for everything except the time-dependent extinction which will be forced to zero. In some cases there were insufficient standard star data to independently determine all terms. Usually in such cases one can adopt a forced value for the color term from a nearby night that had a good determination. Our system does permit forcing the extinction or zero point but this was never done for this project. Nights where such forcing was indicated were simply marked as bad and removed from further consideration.

The transformation relation in Equation (1) follows common methodologies such as Henden & Kaitchuck (1995) except for the time-dependent extinction term. Without this term, some nights show a marked trend in post-fit residuals with time. The true origin of this trend is rarely, if ever, recognized. This term seeks to model the change as a change in the atmospheric extinction. However, a systematic increase or decrease in FWHM through the night can generate a similar signal. Regardless of origin, this term is a first-order correction to a time dependence in the transformation and it corrects some nights that might otherwise be discarded as non-photometric. Two conditions are imposed on the use of this term during data reductions. First, enabling the term must improve the fit. This was recognized as an improvement in the reduced χ^2 as well as a value for η that was significant relative to its uncertainty. The second condition was that science data must not require a substantial extrapolation from the time of the standard star observations. Typical values for η are a few thousandths of a magnitude per hour per airmass. Of the 211 nights of data represented here, 68 required the use of this term.

During the fitting process, the fit and all residuals were visually examined to ensure sensible results. Quite often there were discrepant individual measurements leading to an examination of these apparently bad measurements. There were two

outcomes from this examination: either the measurement was marked bad and excluded from the fit or the bad measurement was an indication that the entire night itself was bad and all data were excluded.

Despite our best efforts to account for all noise sources in the reduction, there remain low-level vagaries in the photometric data. These noise sources could stem from variations in seeing from image to image, subtle transparency variations in Earth’s atmosphere, or perhaps even errors in the standard stars themselves. A good night had a final per-observation scatter of the standard stars of about 1%. This level of scatter seems to represent a lower limit to all-sky absolute photometry based on the Landolt standards. This scatter is never seen to drop as low as 0.5%. At the end of the fit after all bad measurements are excluded we never saw a reduced χ^2 equal to one as it should be if the model and uncertainties are perfectly accurate. Therefore, the final step was to scale all of the uncertainties of the star measurements by $\sqrt{\chi^2}$, thus forcing the final uncertainties on the transformation coefficients to be larger and capture these extra noise sources.

The nightly transformation coefficients are presented in Table 2. There are two entries in this table per night, one for the V filter and one for the R filter (listed under column Fil). All observations were transformed with $(V - R)$ color and thus C_1 is always V and C_2 is always R (first and second filters of the color). This table lists all good nights of observing in chronological order along with all of the transformation coefficients. The column k is the extinction coefficient and σ_k is its uncertainty. Likewise, ϵ stands for the color term coefficient, η for the time-dependent extinction coefficient, JDref is the reference time (t_0), and Z is the zero point (see Equation (1)) each with their own uncertainties. The columns labeled with a subscripted F indicate if the coefficient shown was forced (set to 1) or fitted (set to 0). The column labeled N lists the total number of standard star measurements that were used to constrain the transformation solution. The final column, labeled χ^2 , lists the final goodness-of-fit statistic divided by the number of constraints. This value is prior to the final a posteriori adjustment. The uncertainties for each term include the a posteriori adjustments. A more complete graphical summary and overview of the transformation coefficients for all data is presented in the Appendix.

3.2. Field Star Measurements

The processing of the calibration field images was almost entirely automated. The first step in the processing was to detect discrete sources in the image using Buie library routine `findsrc.pro`. This program searches for positive deviations from the sky background. For this project we used a threshold such that any source with a peak signal higher than 4σ above the sky background would get recorded. This routine also measures and records the object’s FWHM, position, and small-aperture instrumental magnitude using `basphote.pro`. The detection algorithm looks for local maxima in the image over a defined scale called gap, usually set to be the FWHM for the image. The list of sources is also processed to make sure no two sources on the image are closer than gap from each other. Saturated sources are also removed from the list. This routine `findsrc` is comparable in function to the DAOPHOT `find` and `aper` routines (Stetson 1987) but returns a much smaller number of false positives and almost no double detections of the same source.

⁵ This routine and others mentioned in this paper are publicly available at <http://www.boulder.swri.edu/~buie/idl>.

Table 3
Individual Photometric Measurements

Date	Inst.	JD	R.A.	Decl.	Filt	Color	Mag	Err
2001 Aug 26	PCCD	2452147.68148	4.82766686	-0.34520031	R	V-R	13.7278	0.0141
2001 Aug 26	PCCD	2452147.68148	4.82772119	-0.34447472	R	V-R	12.3065	0.0126
2005 Feb 4	SITE2k	2453405.70247	1.50614027	0.39900202	R	V-R	16.0620	0.0048
2005 Feb 4	SITE2k	2453405.70247	1.50614546	0.39857062	R	V-R	16.5282	0.0062
2006 Feb 27	ccd21big	2453794.01672	3.67751991	-0.21684927	R	V-R	16.2210	0.0060
2006 Feb 27	ccd21big	2453794.01672	3.67752896	-0.21708894	R	V-R	16.4000	0.0061
2006 Apr 7	SMARTS	2453832.55132	3.11683206	-0.02950900	R	V-R	18.0923	0.0220
2006 Apr 7	SMARTS	2453832.55132	3.11688534	-0.03288509	R	V-R	11.4668	0.0082
2007 Oct 8	Nasacam	2454381.59740	6.13626705	-0.07663485	R	V-R	16.1920	0.0131
2007 Oct 8	Nasacam	2454381.59740	6.13630793	-0.07842520	R	V-R	17.0836	0.0274

(This table is available in its entirety in a machine-readable form in the online journal. A portion is shown here for guidance regarding its form and content.)

Next, an astrometric solution was derived for each image. The solution was based on USNO B1.0 catalog star positions that were all adjusted to an epoch of 2005. The sky-plane positions of all sources were computed based on the astrometric solution and saved with the information from the first step. The fit for PCCD used a linear mapping from pixel coordinates to tangent plane coordinates. The NASAcam data used a cubic mapping though the high-order terms could probably have been ignored for this project. In all cases, the astrometric errors are limited by the systematics of the USNO B1.0 catalog. These positions are used by us only for source identification, which required stable positions better than 1.5 arcsec, a level easily reached with these procedures.

Each source was then re-measured using the large photometric aperture used for the standard star measurements while forcing the positions to be the same as the positions as determined in the source list extraction step. We made no attempt to identify or remove blended sources.

Determining the absolute magnitude of each source requires the simultaneous determination of its standard color. On a field by field basis, the source lists for a given field are cross-correlated to generate a list of unique sources. This correlation was done on the astrometrically determined positions and is thus not sensitive to any shifts in image pointing between successive frames. The set of measurements for a given source are then processed together to solve for the mean color from the set and thus determine the final measured absolute magnitude given the transformation coefficients for the night. Table 3 contains a complete listing of all individual source measurements from all good nights of data. The R.A. and Decl. columns are both given in radians.

4. CATALOG

The final step in the creation of the photometric catalog is to combine observations from multiple nights and generate the final average magnitudes for each star. To ensure a unique collation of sources into the final catalog a sky grid was created. This grid consists of 3 arcsec square tiles over the entire sky. This grid is then numbered consecutively east from 0 hr right ascension within its declination band. The declination bands are numbered relative to the equator, positive for north and negative for south. This pair of numbers was converted to a zero-padded string and the source in the tile is then named for this identifying string. Converting the identification string back to right ascension and declination will result in a position that is within 1.5 arcsec of the actual position of the source. The

size of the tile was set for the typical spatial resolution from the images. The seeing limit combined with the source detection algorithm leads to a clean mapping from source lists to a final object identification.

Once the individual measurements are correlated using the object identifier, it becomes a simple matter to average the positions and magnitudes. Table 4 contains the final result of this averaging process. The identifier listed in the first column is the string described in the previous paragraph. The position (α , δ) is given in radians, the uncertainties (σ_α and σ_δ) are in arcseconds and represent the standard deviation of the mean from averaging the positions. N stands for the number of measurements and N_i stands for the number of independent nights. The final uncertainties tabulated for the photometry of each source are the larger of the error in the mean from the individual measurements or the propagated uncertainties from the individual errors.

Our goal was to collect observations from three nights for every star in the catalog but this was not possible in the end. In the final catalog there are a total of 213,272 individual sources tabulated. Of these, 35,427 sources were measured on three or more nights and 58,199 sources were measured on two nights. Also included in this table is a calculated SDSS r' magnitude and ($g' - r'$) color. We used the transformation coefficients from Smith et al. (2002) for these values and this is the calibration upon which the DES data are based. New transformation relationships between the Johnson-Cousins system and the SDSS system would clearly take precedence over our numbers. Such improvements are unlikely to affect the DES results since the calibration of those data is hampered by the lack of any color information from which to base the transformation.

A rough idea of the magnitude range covered by the catalog is shown in Figures 1 and 2. Most of the sources are in the 16–17 mag range for V and 15–16 mag range for R . The falloff in number of sources with decreasing brightness is caused by the intrinsic flux limit of our observations. Figure 3 summarizes the range of ($V - R$) color in the catalog sources. A very small number of sources are extremely blue or extremely red but were omitted from this histogram. In general, this distribution of stars provides a very good color range for calibrating solar system objects. Figure 4 presents a summary of the typical uncertainties in the catalog, shown here for the R magnitudes. The sources fainter than $R = 14$ generally show an increase in their uncertainties with decreasing brightness as would be expected from our fixed exposure durations.

The application of this photometric catalog to the DES data takes advantage of every source possible. Through the

Table 4
DES Photometric Support Catalog

ID	R.A.(α)	Decl.(δ)	σ_α	σ_δ	V	σ_V	R	σ_R	$(V - R)$	$\sigma_{(V-R)}$	N_V	N_R	Nbad	Ni $_V$	Ni $_R$	r'	σ_r	$(g' - r')$	σ_{g-r}
0000444-005291	0.00648324	-0.07694935	0.001	0.001	18.4082	0.0334	17.5622	0.0214	0.8460	0.0397	3	4	0	1	1	17.8768	0.0288	1.6203	0.0517
0000444-005491	0.00647380	-0.07986123	0.001	0.004	16.2093	0.0101	15.7505	0.0086	0.4588	0.0133	9	12	0	3	3	15.9733	0.0108	0.9641	0.0173
0000444-005517	0.00647230	-0.08024140	0.001	0.001	16.8249	0.0085	16.2149	0.0021	0.6100	0.0087	3	4	0	1	1	16.4735	0.0047	1.2203	0.0113
0000445+004405	0.00648902	0.06406754	0.006	0.005	13.7704	0.0029	13.3953	0.0034	0.3750	0.0045	12	16	0	4	4	13.5982	0.0040	0.8220	0.0059
0000448+004440	0.00652995	0.06457359	0.003	0.012	16.8712	0.0280	16.5875	0.0202	0.2837	0.0345	9	12	0	3	3	16.7687	0.0263	0.6673	0.0449
0000449+004491	0.00654764	0.06531186	0.005	0.007	16.6356	0.0115	16.2452	0.0148	0.3903	0.0187	9	12	0	3	3	16.4517	0.0174	0.8480	0.0243

Notes. “ID” is the internal source identifier used. The source position is given by R.A. and decl. (in radians). The uncertainty on the position is given by σ_α and σ_δ . The V and R magnitudes and their uncertainties are given in the next four columns. The color used during photometric transformation and its uncertainty is given in the next two columns. “ N_V ” is the number of V -band measurements. “ N_R ” is the number of R -band measurements. “Nbad” is the number of observations in either filter marked as bad. “Ni $_V$ ” is the total number of independent nights in the final measurements for the V data. “Ni $_R$ ” is the total number of independent nights in the final measurements for the R data. The last four columns give the SDSS r' magnitude and $(g' - r')$ color and propagated uncertainty derived from the original V and R measurements.

(This table is available in its entirety in a machine-readable form in the online journal. A portion is shown here for guidance regarding its form and content.)

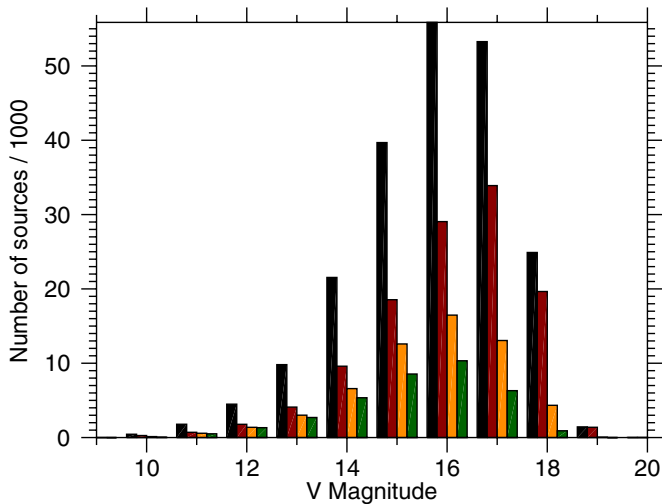


Figure 1. Histogram of the V magnitude measurements in the final catalog. The left-most bar for each bin is the distribution of the entire catalog. The second (red) bar is for those objects measured only on one night. The third (orange) bar is for those objects measured on two nights. The fourth (green) bar is for those objects measured on three or more nights.

(A color version of this figure is available in the online journal.)

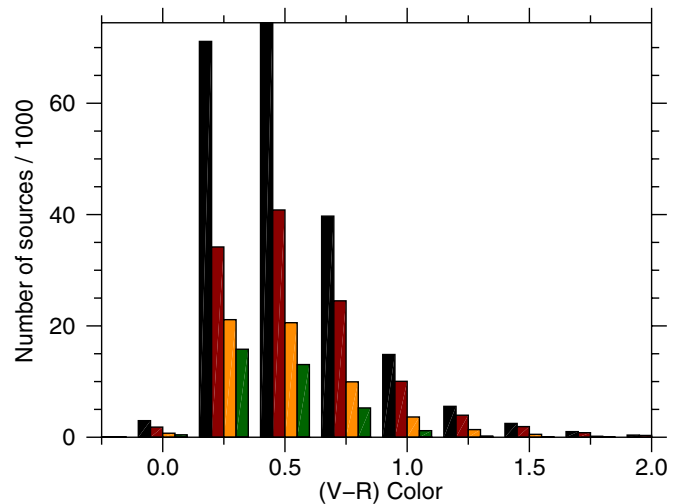


Figure 3. Histogram of the $(V - R)$ color measurements in the final catalog. The left-most bar for each bin is the distribution of the entire catalog. The second (red) bar is for those objects measured only on one night. The third (orange) bar is for those objects measured on two nights. The fourth (green) bar is for those objects measured on three or more nights.

(A color version of this figure is available in the online journal.)

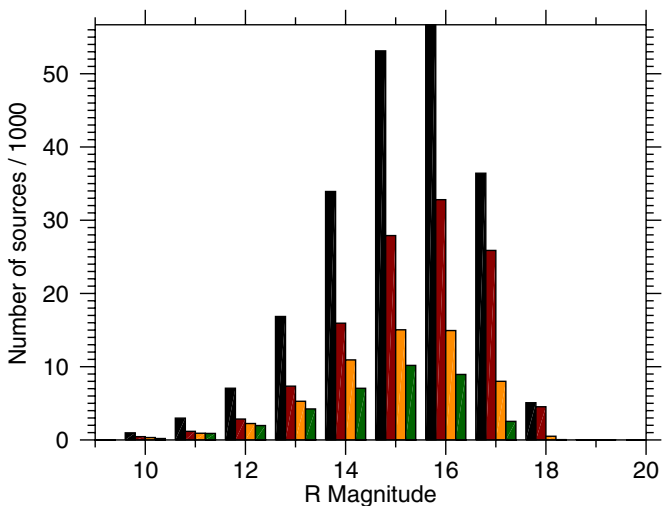


Figure 2. Histogram of the R magnitude measurements in the final catalog. The left-most bar for each bin is the distribution of the entire catalog. The second (red) bar is for those objects measured only on one night. The third (orange) bar is for those objects measured on two nights. The fourth (green) bar is for those objects measured on three or more nights.

(A color version of this figure is available in the online journal.)

use of multiple stars it is very easy to achieve a calibration of the image limiting magnitude good to 10%, even with the faintest stars in this catalog. The photometry data are processed with little supervision and have not been filtered to remove variable stars or stars that are contaminated by close companions though unusually large uncertainties will be a key indicator of problems. It is very important to use as many stars as possible—10 is not an unreasonable number—so that statistical outliers can be identified and removed from the ensemble zero-point determination when calibrating an image. This warning is especially important if the image quality differs significantly from that achieved during these observations (nominally $\text{FWHM} = 3''\text{--}4''$).

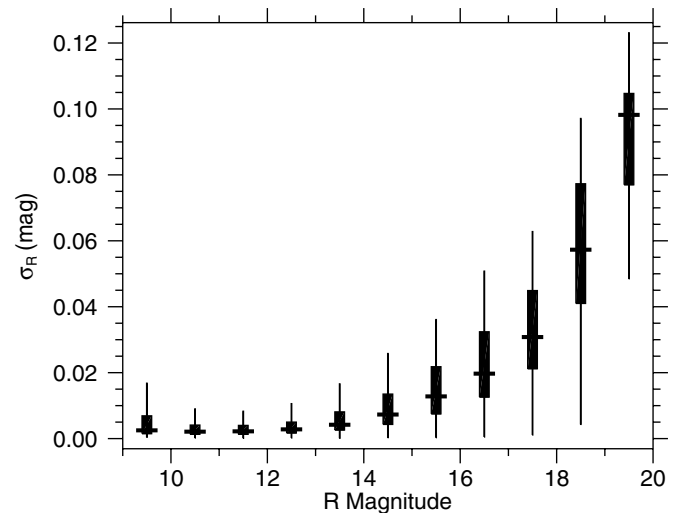


Figure 4. Summary plot of the uncertainties on the R measurements. The symbols for each magnitude show the minimum error up to the 90% percentile error with the thin vertical bar. The heavy vertical rectangle shows the error range from the first to last quartile of the error range. The wide horizontal bar shows the median of the errors in that bin.

5. CONCLUSIONS

The final photometric catalog meets the needs of the DES by providing absolute calibration of its limiting magnitudes as well as source fluxes to better than 10%. In most cases, the calibration is considerably better than this requirement—often as good as 3%. This project would have been impossible without a substantial contribution from robotic telescope operations. We anticipate that these photometric observations will be useful to others.

This paper is based on observations taken at Lowell Observatory, CTIO-SMARTS, and the University of Arizona 1.5 m Kuiper Telescope. Support for this work was provided by NASA and NSF through grant numbers NNG06-GI23G and AST-0407232/0454044/0950631. Support for R.A.C. was also

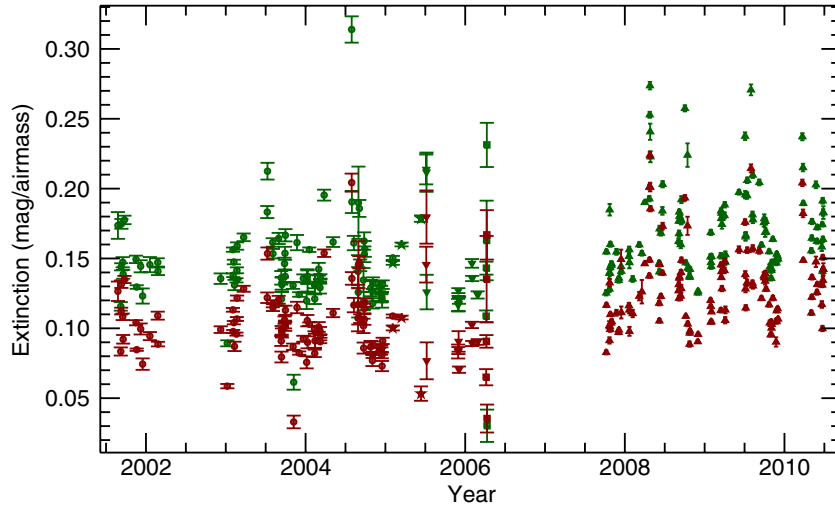


Figure 5. Extinction coefficients for all nights. The green symbols show the V extinction and red symbols show the R extinction for all nights in our data set. Data prior to early 2005 is from the early PCCD system. Data in late 2005 and early 2006 are from other facilities in Arizona and Chile. Data from late 2007 onward are from the newer NASAcam instrument at Lowell.

(A color version of this figure is available in the online journal.)

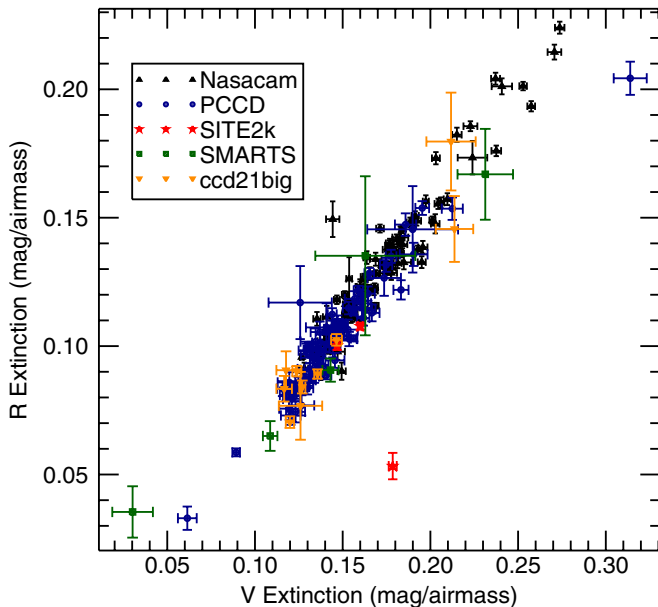


Figure 6. Relationship between V and R extinction. The R extinction is plotted vs. V extinction for each night of data. These results show a very tight correlation between the two extinction coefficients.

(A color version of this figure is available in the online journal.)

provided by the NASA Space grant program at the University of Arizona.

APPENDIX

PHOTOMETRIC TRANSFORMATION VALUES AND TRENDS

Having a large collection of data on many photometric nights permits seeing interesting and sometimes useful trends in the photometric transformation coefficients. The following figures provide a graphical summary of the information contained within Table 2.

Figure 5 contains a summary of extinction (k from Equation (1)) in V (green) and R (red). There is very little to distinguish the different instruments, telescopes, and sites used in this study. In general, the V extinction is seen to fall in the range of 0.13 to 0.20 with some excursions above and below. The R extinction is seen to be systematically lower, as expected, and ranges from roughly 0.07 to 0.15. Within this general range you can clearly see significant short-term variations that can exceed a factor of two in a matter of days. The most recent data show significantly smaller uncertainties thanks to the larger field-of-view (more standard stars) and lower read-noise.

There is a strong correlation between V and R extinction that is shown in Figure 6. The tightest grouping comes from the lower noise NASAcam observation but all of the cameras fall along this trend. Very few points deviate from the general linear trend. However, there is still meaningful scatter within the trend arguing strongly that independent extinction measurements are needed for both filters each night.

Figure 7 shows all of the color term determinations in the data set for both filters. All cameras show a larger, more negative color term in R than in V . The newer NASAcam data show a markedly larger color term than all other cameras. The filters are stock Bessell VR filters from Omega and the earlier PCCD filters were also claimed to be based on the Bessell formulation. Apparently following this formula is insufficient to ensure small color terms or the actual manufacturing process has changed the result.

The zero-point trend is shown in Figure 8. The two longest time bases shown are for the PCCD (early) and NASAcam (late) cameras. These curves are dominated by the evolution of the primary and secondary mirror coatings. The larger offset between these two cameras shows the difference in quantum efficiency between a thick front-side illuminated CCD (PCCD) and a thinned back-side illuminated CCD (NASAcam). The differences for the other systems are largely dominated by the size of the telescope. The visibility of these general trends is an important cross-check on the overall integrity of the photometric calibration.

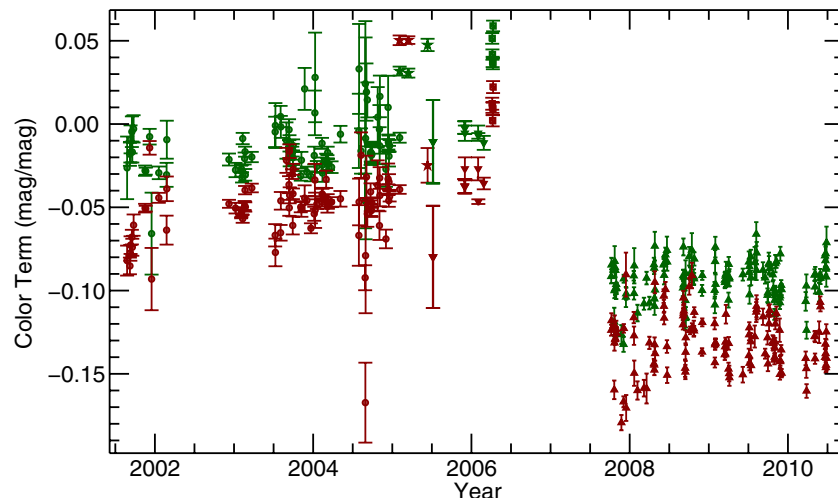


Figure 7. Color term trends and comparisons between cameras. The green symbols show the V color term and red symbols show the R color term for all nights in our data set. Data prior to early 2005 are from the early PCCD system. Data in late 2005 and early 2006 are from other facilities in Arizona and Chile. Data from late 2007 onward are from the newer NASAcam instrument at Lowell.

(A color version of this figure is available in the online journal.)

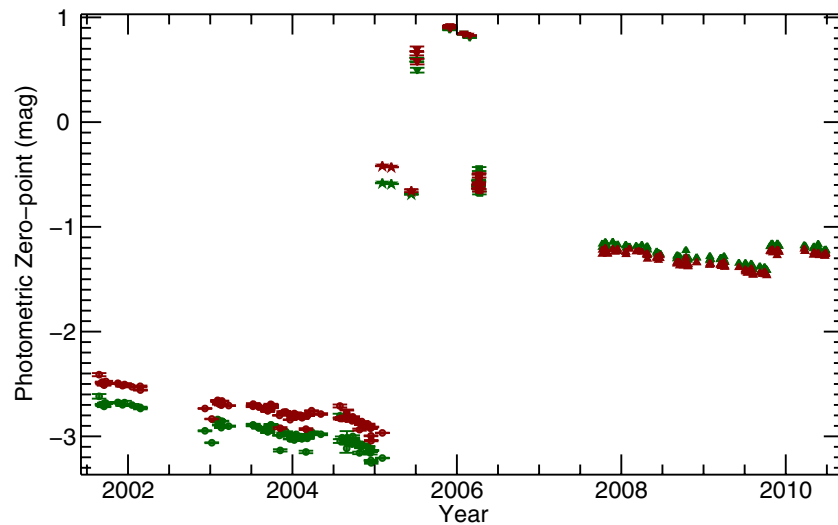


Figure 8. Zero-point trends and comparisons between cameras and telescopes. The green symbols show the V zero point and red symbols show the R zero point for all nights in our data set. Data prior to early 2005 are from the early PCCD system. Data in late 2005 and early 2006 are from other facilities in Arizona and Chile. Data from late 2007 onward are from the newer NASAcam instrument at Lowell.

REFERENCES

- Adelman-McCarthy, J. K., et al. 2006, *ApJS*, **162**, 38
- Brucker, M. J., Grundy, W. M., Stansberry, J. A., Spencer, J. R., Sheppard, S. S., Chiang, E. I., & Buie, M. W. 2009, *Icarus*, **201**, 284
- Buie, M. W. 2010, *Adv. Astron.*, **2010**, 130172
- Buie, M. W., & Bus, S. J. 1992, *Icarus*, **100**, 288
- Elliot, J. L., et al. 2005, *AJ*, **129**, 1117
- Henden, A. A., & Kaitchuck, R. H. 1990, *Astronomical Photometry* (Richmond, VA: Willman-Bell)
- Landolt, A. U. 1992, *AJ*, **104**, 340
- Millis, R. L., Buie, M. W., Wasserman, L. H., Elliot, J. L., Kern, S. D., & Wagner, R. M. 2002, *AJ*, **123**, 2083
- Smith, J. A., et al. 2002, *AJ*, **123**, 2121
- Stephens, D. C., & Noll, K. S. 2006, *AJ*, **131**, 1142
- Stetson, P. B. 1987, *PASP*, **99**, 191